applied sciences

MDPI

Article

Quantitative Analysis of Basalt Damage Under Microwave Radiation Utilizing Uniaxial Compression and Nuclear Magnetic Resonance (NMR) Experiments

Tubing Yin, Jihao Wang *, Jiexin Ma, Jianfei Lu and Hao Dai

School of Resources and Safety Engineering, Central South University, Changsha 410017, China
* Correspondence: 225511024@csu.edu.cn

Abstract: Microwave-assisted rock breaking is recognized as an effective technology for reducing tool wear and enhancing rock-breaking efficiency. In this study, basalt rock was irradiated with a microwave power of 3 kW and 6 kW for 30 s, 60 s, 90 s, and 120 s. Subsequently, uniaxial compression, uniaxial loading and unloading, and acoustic emission tests were performed. The damage evolution of basalt was assessed through non-destructive acoustic testing methods and nuclear magnetic resonance (NMR) techniques. The results showed that the P-wave velocity, uniaxial compressive strength (UCS), and modulus of elasticity (E) exhibited varying degrees of deterioration as the microwave radiation time increased. An increase in microwave radiation time and power led to heightened acoustic emission activity in basalt and a significant rise in the proportion of shear cracks during uniaxial compression. From an energy perspective, microwave irradiation decreased the energy storage capacity of the basalt specimen prior to its peak point, with increased power and duration. At a microscopic level, porosity and the macroporous fractal dimension increased with extended microwave radiation time and power, indicating that microwave irradiation facilitated the growth of larger fractal pore structures. The findings of this study offer scientific insights for the application of microwave-assisted rock crushing.

Keywords: microwave radiation; nuclear magnetic resonance (NMR); acoustic emission; macroporous fractal dimension

Academic Editor: Nico P. Avdelidis

Received: 13 November 2024
Revised: 5 December 2024
Accepted: 22 December 2024
Published: 24 December 2024

Citation: Yin, T.; Wang, J.; Ma, J.; Lu, J.; Dai, H. Quantitative Analysis of Basalt Damage Under Microwave Radiation Utilizing Uniaxial Compression and Nuclear Magnetic Resonance (NMR) Experiments. *Appl. Sci.* **2025**, *15*, 31. https://doi.org/10.3390/app15010031

1. Introduction

In recent years, with the advancement of economic globalization, the mining industry has become a cornerstone of national economic development [1]. In 2023, the sector encountered both new opportunities and significant challenges, particularly in the areas of environmental protection and technological innovation. As mining operations extend to greater depths [2,3], traditional blasting techniques have struggled to adapt to the increasingly complex conditions posed by high ground pressure, elevated temperatures, and the rising demands for environmentally friendly, safe, and efficient mining practices [4–7]. In deep mining, the required blasting intensity surpasses that of shallower operations. The substantial elastic deformation energy accumulated in deep rock masses can easily lead to engineering disasters, such as rock bursts and induced seismicity, due to the destabilizing effects of blast-induced rock fracturing [8,9].

Currently, mechanized mining of ores is widely adopted, offering substantial advantages over traditional blasting methods, such as environmental sustainability, improved safety, minimal mining disturbances, high precision, and the capacity for continuous operation [10–13]. However, tool wear during rock excavation often results in increased costs and

reduced efficiency [14]. In response, recent advancements in rock-breaking technologies, including high-pressure water jets, microwaves, lasers, and electron beams, have been introduced into mining operations [15–19]. Among these, microwave irradiation, which can weaken or even destroy rock strength, is considered a promising non-explosive mining method due to its precision, cost-effectiveness, and alignment with green mining principles.

The use of microwaves for rock weakening has become a prevalent trend and focus of research in rock-breaking technologies. Researchers have explored the effects of microwave irradiation on rocks by evaluating changes in their physical and mechanical properties post-exposure. Hassani [20] reported that the tensile strength of basalt specimens decreased from 12 MPa to 8 MPa when the irradiation duration was increased from 10 to 20 s at a power level of 5 kW. Similarly, Kingman [21] demonstrated that when using a multimode cavity microwave device at 15 kW, the point load strength of ore specimens decreased by 55% after just one second of exposure. Lu [22,23] found that the longitudinal wave velocity in cubic rocks with 20 cm sides decreased by 2.2%, 6.0%, and 8.4% after irradiation times of 5, 10, and 15 min at 3 kW, respectively. Toifl et al. [24–26] studied the effects of microwave irradiation on the mechanical and thermodynamic properties of granite, sandstone, and basalt. Energy-based studies, such as those by Jones [27], Monti [28], and John [29], have conducted extensive experiments and simulations demonstrating a significant reduction in the Bond's work index of rocks after microwave treatment. Jian-ming Yang [30] concluded that the energy storage limit and residual elastic energy density of granite are inversely proportional to the power and duration of irradiation. Collectively, these findings highlight that microwave irradiation effectively weakens rock strength.

The absorption capacity of minerals within rocks for microwaves is primarily determined by their dielectric constants; minerals with higher dielectric constants absorb microwaves more efficiently, resulting in more rapid temperature increases. Due to the variation in dielectric constants among different minerals in a rock, some minerals heat faster under microwave radiation, while others heat more slowly, creating temperature gradients within the rock. This differential heating, combined with the varying expansion rates of minerals, induces thermal stresses that cause both inter-crystal and intra-crystal fractures, as illustrated in Figure 1. Compared to other rock damage methods, microwave radiation is characterized by two critical parameters: power and duration. Understanding the distinct effects of these parameters on rock deterioration is crucial for the practical application of microwave-assisted rock breaking in mining. Yin et al. [31] reported that higher microwave power and longer irradiation times exacerbate basalt damage, with faster surface temperature increases correlating with reductions in both dynamic compressive strength and longitudinal wave velocity, alongside increases in peak strain. Kingman [32,33] emphasized that a rock's mineral composition significantly affects its sensitivity to microwaves, underscoring the importance of optimizing power and duration settings for effective microwave-assisted rock breaking. Merely increasing microwave power does not guarantee optimal outcomes in rock breaking. In related studies, Satish et al. [34] examined the effects of microwave heating on basalt and observed excellent microwave absorption properties, significantly reducing the energy required for mechanical cutting. Microwave irradiation not only rapidly heats the rock but also induces thermal stresses that initiate and propagate fissures, enhancing rock cutability by significantly reducing wave velocity, increasing porosity, and lowering dynamic compressive strength.

Currently, numerous researchers have investigated the effects of thermal stress on rocks by altering microwave powers through static and dynamic loading. However, there remains a significant gap in the quantitative analysis of the damage caused by microwave radiation to basalt, particularly concerning pore distribution and internal strain energy density. To address this gap, the primary objective of this study is to employ Nuclear Magnetic

Resonance (NMR) and uniaxial static compression experiments to systematically examine the changes in the pore structure and energy density of basalt subjected to microwave radiation. Through this research, we aim to provide valuable insights that will contribute to the advancement of materials engineering, particularly in optimizing microwave treatment techniques for improved rock performance.

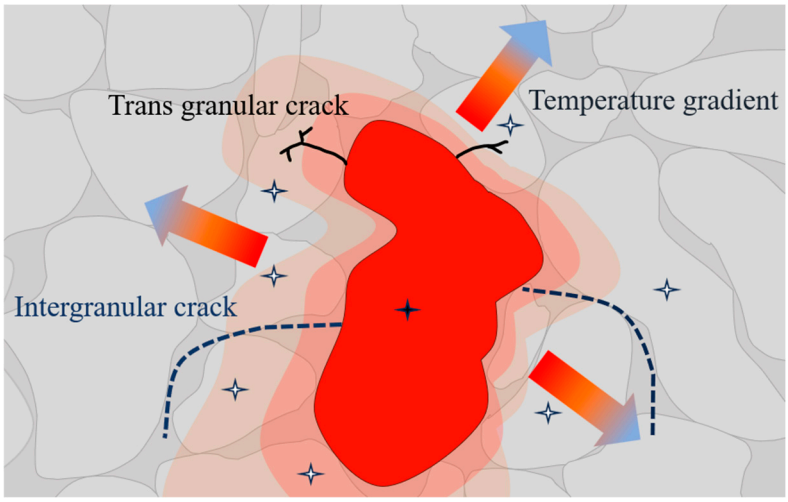

Figure 1. Schematic diagram of damage mechanism of basalt under microwave radiation (represents microwave-sensitive mineral; represents microwave-insensitive mineral).

2. Experimental Method

2.1. Material Description and Sample Preparation

Basalt, an igneous rock rich in iron and magnesium, is widely distributed across the globe. Its primary mineral components, pyroxene and plagioclase, exhibit dipolar properties that are particularly significant under microwave radiation. When exposed to microwave radiation, the electric field interacts with these dipolar minerals, causing rapid vibrational movements that generate heat. As a result, basalt exhibits a highly responsive behavior to microwave irradiation. For this study, fine-grained basalt was sourced from Wutai County, Shanxi, China. The specimens were extracted from the same fresh rock mass and shaped into cylinders with a diameter of 50 mm and a height of 100 mm, following the standards recommended by the International Society for Rock Mechanics (ISRM). The ends of each specimen were polished to ensure parallelism with an accuracy of ± 0.05 mm and a surface roughness of less than 0.02 mm. The physical properties of these specimens are presented in Table 1. X-ray diffraction (XRD) analysis of the mineralogical composition revealed that the basalt used in the experiments consisted primarily of mesquite feldspar (59.33%), pyroxene (26.84%), olivine (11.95%), and ilmenite (1.88%), as illustrated in Figure 2.

Table 1. Rock mechanical parameters of basalt specimens at room temperature (25 °C).

	Longitudinal Wave Velocity, V/(m·s^{-1})	**Density, ρ/(g·cm^{-3})**	**Compressive Strength, σ_c/Mpa**	**Modulus of Elasticity, E (Gpa)**	**Poisson's Ratio, μ**
Specimen 1	5850.7	2.91	103.99	30.48	0.21
Specimen 2	5716.5	2.89	102.25	30.31	0.23
Average	5783.6	2.90	103.12	30.39	0.22
Standard deviation	94.894	0.014	1.230	0.120	0.007

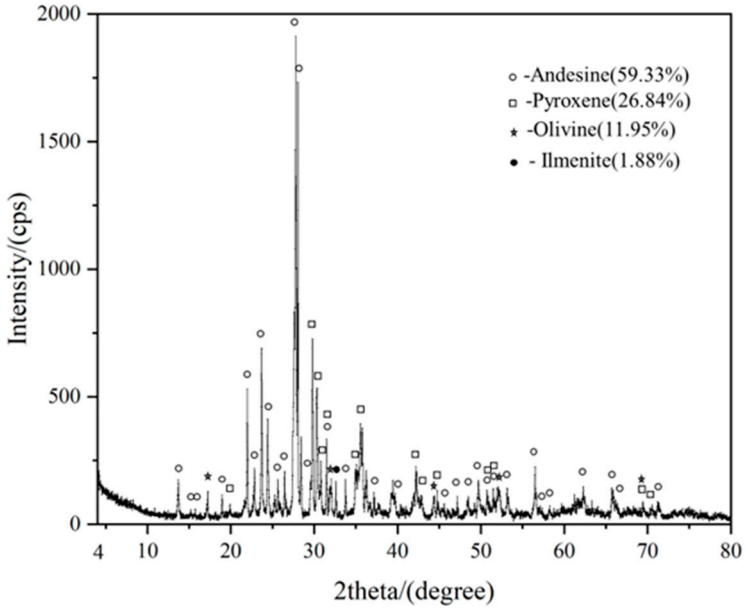

Figure 2. XRD pattern of basalt.

2.2. Microwave Heating Steps and Procedures

Experiments were conducted using a WLKJ-A9 multi-film cavity industrial microwave oven (2.45 GHz, 15 kW), provided by Central South University. Microwave radiation power settings of 0, 3, and 6 kW were applied, with irradiation durations of 30, 60, 90, and 120 s, resulting in a total of nine experimental groups. Each group consisted of five rock specimens, with two designated for uniaxial compression tests and three for cyclic loading and unloading tests, amounting to a total of 45 specimens. After irradiation, the specimens were cooled at room temperature (25 °C). The post-cooling rock specimens are shown in Figure 3. Measurements of mass and wave velocity were taken before and after microwave irradiation. In addition, the pore distribution and mechanical properties of the cooled specimens were analyzed using a Niumag AniMR-150 nuclear magnetic resonance (NMR) system (Niumag Company in China) and an Instron 1346 electro-hydraulic servo universal testing machine (Instron Company in the UK), both depicted in Figure 3.

Nuclear Magnetic Resonance (NMR) techniques provide an advanced, non-destructive way to measure rock porosity by analyzing the magnetic properties of certain nuclei, particularly hydrogen [35–37]. When rocks containing water are placed in a strong magnetic field, the hydrogen nuclei in the water molecules align with the field. A radio frequency (RF) pulse is then applied, temporarily disrupting this alignment. As the hydrogen nuclei return to their original state, they release energy, which is detected as an NMR signal. This signal gives valuable information about the pore structure of the rock, especially in small pores or rocks with low porosity. Since NMR is sensitive to hydrogen in water, it can effectively assess changes in porosity without damaging the sample, allowing for repeated measurements over time. The principle of NMR signal release is shown in Figure 4.

For the specific purpose of measuring basalt porosity following microwave treatment, the basalt specimens in this study were first saturated by soaking in water for two days. This saturation ensures that the pores within the basalt are completely filled with water, thereby maximizing the NMR signal from the hydrogen nuclei. After saturation, to prevent water loss and maintain the saturated state during measurement, each specimen was carefully wrapped in cling film before being placed in the NMR instrument. Once the RF pulse is switched off, the NMR instrument detects the RF signals emitted during the nuclei's relaxation process. This approach enables the precise measurement of changes in

the pore structure caused by microwave radiation, providing valuable insights into the effects of microwave treatment on the physical properties of basalt.

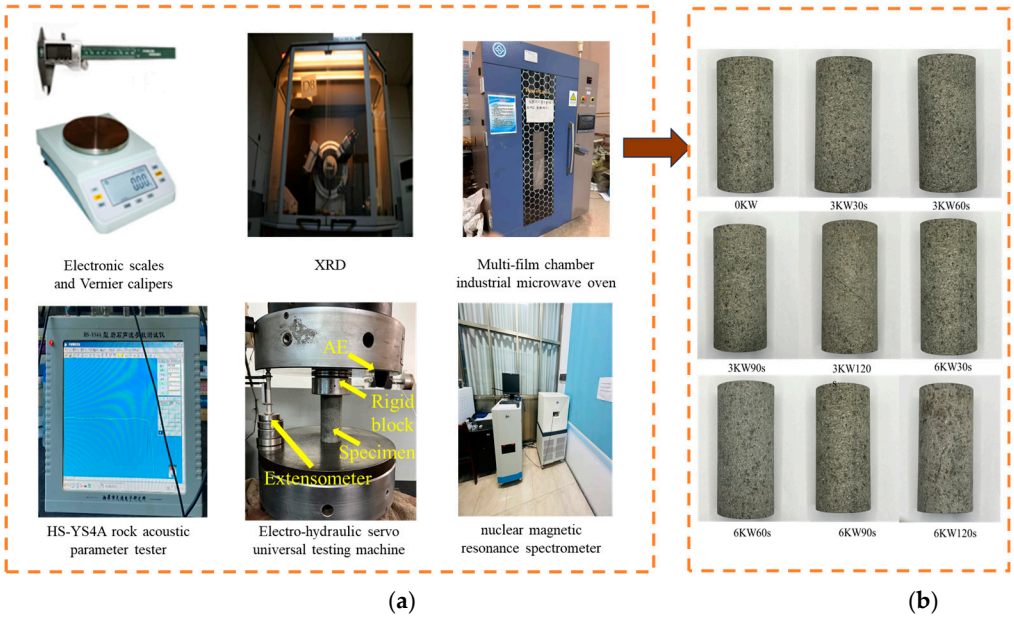

Figure 3. Experimental instruments with microwave radiation after the sample. (**a**) Experimental equipment. (**b**) Basalt sample after microwave irradiation.

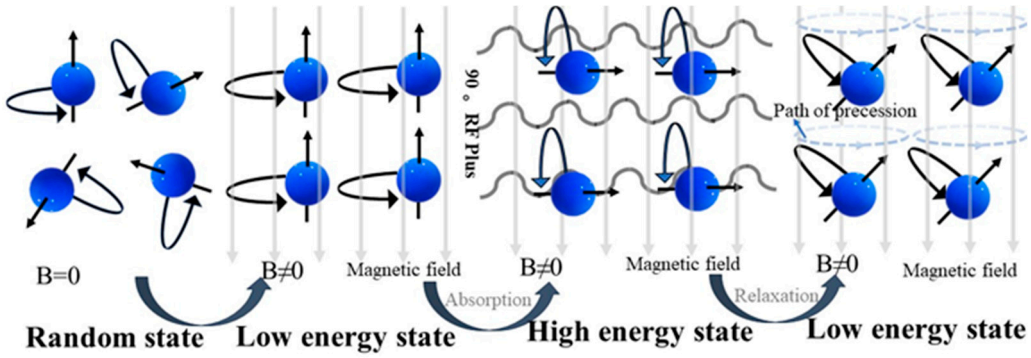

Figure 4. Principle of NMR signal release.

3. Results

3.1. Changes in Wave Velocity of Specimens After Microwave Treatment

The propagation of ultrasonic waves within rock is significantly affected by its fracture structure. When ultrasonic waves encounter fissures, they are partially reflected or refracted, which alters both their path and speed. Therefore, by analyzing the propagation characteristics of ultrasonic waves in rock, internal fissures can be inferred, offering a macroscopic evaluation of the rock's structural integrity and properties. The experiment utilized the HS-YS4A rock acoustic parameter tester, which supports a frequency range of 100 kHz to 20 MHz. This device was manufactured by the Xiangtan Electronic Research Institute, China. This instrument is equipped with a cylindrical ultrasonic transducer, enhancing its capability to accurately measure acoustic parameters in various rock samples. Ultrasonic measurements were conducted on different groups of basalt using a sampling frequency of 10 MHz to determine the wave velocity. Data showing substantial velocity variances were excluded, and the wave velocities of the remaining specimens were averaged, as presented in Table 2.

Table 2. Damage coefficients F_D and longitudinal wave velocity of basalt samples under different microwave radiation power and time.

Microwave Power	Microwave Radiation Duration	Average Longitudinal Wave Velocity, V/(m/s)	Average Damage Coefficient F_D	Standard Deviation of F_D
0 kW	0 s	5783.6	0	0.0328
3 kW	30 s	5647.2	0.046612	0.0308
	60 s	5313.6	0.155925	0.0310
	90 s	5053.2	0.236628	0.0302
	120 s	4915.8	0.277576	0.0280
6 kW	30 s	5388.1	0.132090	0.0331
	60 s	4635.2	0.357682	0.0274
	90 s	4224.4	0.466501	0.0237
	120 s	4121.8	0.493579	0.0230

After absorbing 3 kW and 6 kW of microwave energy, the basalt specimens displayed a pattern where the rate of wave speed reduction initially intensified before diminishing, as shown in Figure 5. This pattern occurs because, at the beginning of microwave exposure, the rock absorbs microwave energy, leading to increased water evaporation and accelerated mineral decomposition. The associated temperature rise induces thermal stress within the rock, causing the formation and expansion of microcracks, which in turn accelerates the decline in wave speed. However, once the intensity and duration of microwave radiation surpass certain thresholds, the internal damage to the rock reaches a critical state, causing the rate of wave velocity reduction to peak before rapidly decreasing. This decline is due to the extensive damage, which reduces the rock's efficiency in absorbing further microwave energy. In this study, longitudinal wave velocity is used to quantitatively characterize the damage in microwave-treated rock specimens [38]. The damage coefficient is defined as follows:

$$F_D = 1 - \left(\frac{V_P^{post}}{V_P^{pre}}\right)^2 \quad (1)$$

In this context, V_P^{pre} represents the longitudinal wave velocity of the rock specimen before microwave treatment, and V_P^{post} represents the longitudinal wave velocity of the rock specimen after microwave treatment. The damage coefficient is calculated to quantify the extent of damage induced by microwave radiation. The closer the damage coefficient is to 1, the greater the damage inflicted on the rock specimen by the microwave treatment. The results, as shown in Table 2, illustrate the relationship between microwave exposure and rock deterioration based on this damage coefficient.

Under 3 kW of microwave radiation, the damage coefficient of the specimen after 30 s of irradiation is only 29.89% of that after 60 s, whereas the damage coefficient after 90 s reaches 85.25% of that after 120 s. Similarly, under 6 kW of microwave radiation, the damage coefficient after 30 s is 36.93% of that after 60 s, while the damage coefficient after 90 s reaches 94.51% of that after 120 s. These results demonstrate the progressive nature of damage as irradiation time increases, with higher power levels significantly accelerating the accumulation of damage. Furthermore, the extent of damage to basalt follows a pattern where the rate of damage initially intensifies and then diminishes as the irradiation duration is extended.

This section may be divided by subheadings. It should provide a concise and precise description of the experimental results, their interpretation, as well as the experimental conclusions that can be drawn.

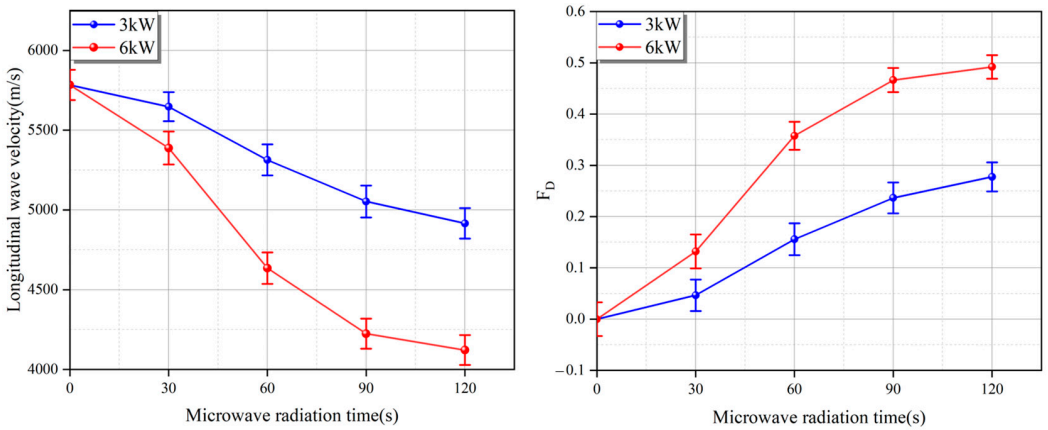

Figure 5. (**a**) Changes in longitudinal wave velocity in microwave-treated rocks. (**b**) Variation in the value of F_D with different microwave radiation.

3.2. Characteristic of Pore Space Variations in the Interior of Rocks Using NMR

The T_2 relaxation time in Nuclear Magnetic Resonance (NMR) spectroscopy is a key parameter that is directly influenced by the size, shape, and surface characteristics of the pores where the hydrogen nuclei reside. In porous materials like rocks, larger pores generally result in longer T_2 relaxation times due to slower dephasing of nuclear spins, whereas smaller pores correspond to shorter T_2 relaxation times because of faster dephasing caused by the increased surface area-to-volume ratio.

In the present research, pores larger than 0.1 μm are classified as macropores, whereas pores smaller than 0.1 μm are designated as small pores. The 0 kW condition is defined as the basalt specimens that have not been subjected to microwave radiation treatment. As demonstrated in Table 3, the Nuclear Magnetic Resonance (NMR) results reveal a progressive increase in porosity within the basalt specimens, corresponding to both the duration and power of microwave radiation applied. This phenomenon can be attributed to microwave radiation facilitating the formation of additional microcracks and pores within the rock's microstructure. The observed increase in porosity, coupled with changes in pore distribution, serves as a robust indicator of microwave-induced damage to the basalt, as illustrated in Figure 6. For example, the porosity of the basalt specimen after 120 s of 6 kW microwave radiation increased by 0.3496% compared to the untreated basalt, while the porosity after 120 s of 3 kW microwave radiation increased by 0.1899% compared to the untreated specimen. Additionally, it is evident that basalt subjected to 6 kW microwave radiation experienced a more significant increase in porosity compared to that subjected to 3 kW radiation. Specifically, the porosity of the basalt after 120 s of 6 kW microwave radiation increased by 0.1597% compared to that after 120 s of 3 kW microwave radiation.

Table 3. The porosity of basalt samples after different microwave radiation.

Microwave Power	Microwave Radiation Duration	Porosity (%)
0 kW	0 s	0.9099
3 kW	30 s	0.9701
	60 s	1.0401
	90 s	1.0893
	120 s	1.0998
6 kW	30 s	0.9824
	60 s	1.2002
	90 s	1.2494
	120 s	1.2595

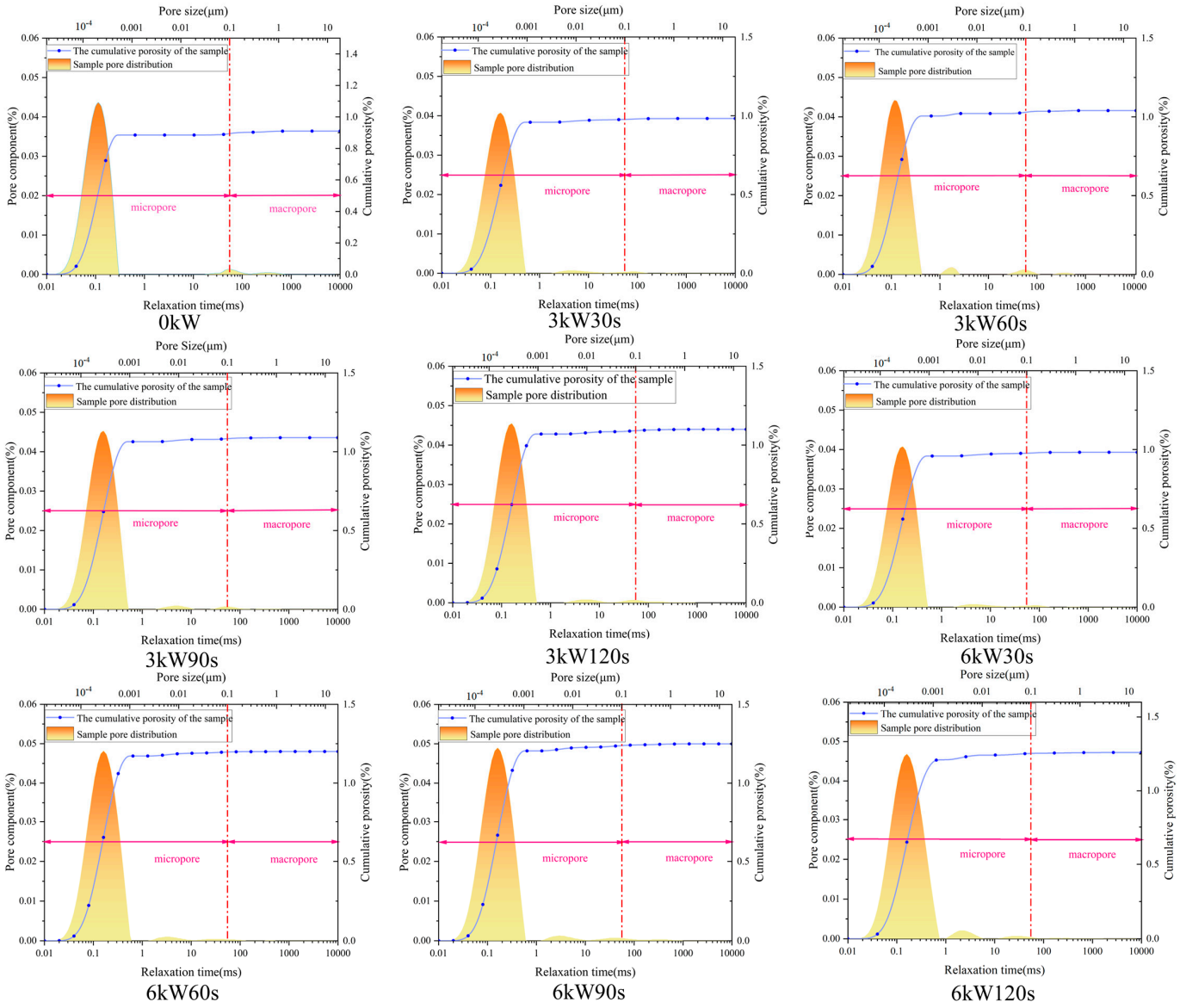

Figure 6. Pore size distribution of basalt samples after different microwave radiation.

3.3. Effect of Microwave Radiation on Mechanical Properties of Basalt Specimens Based on Uniaxial Experiments

The stress–strain curves obtained from uniaxial compression tests on basalt typically exhibit four distinct stages: microcrack compaction, elastic deformation, microcrack expansion, and post-destruction. These stages can be characterized as follows:

(1) Microcrack Compaction Stage: During the initial loading phase, pre-existing defects within the specimen gradually close under external stress, accompanied by the formation of a few new microcracks. This stage is marked by a nonlinear stress–strain curve, where relatively large applied stress causes minimal deformation, indicating the compaction effect resulting from initial inhomogeneity. The deformation in this stage is predominantly reversible and elastic.

(2) Elastic Deformation Stage: Once the pre-existing defects are fully closed, the material enters a stage of clear linear elastic behavior, where the stress is proportional to the strain. The elastic modulus of the rock is determined from the slope of the curve during this stage, and the deformation remains reversible and elastic.

(3) Microcrack Expansion Stage: As the stress continues to increase, new microcracks form, and existing cracks begin to extend and interconnect, resulting in increased

plastic deformation. The stress–strain relationship becomes non-proportional, and the slope of the curve decreases, reflecting a reduction in the rock's deformation modulus.

(4) Post-Destructive Stage: After reaching the peak stress, the primary load-bearing structure of the rock is severely compromised by the continued expansion of cracks, leading to rapid failure of the specimen. The curve shows a sharp drop in stress, followed by a significant increase in strain, eventually resulting in rupture.

As presented in Table 4, it is evident that microwave radiation reduces both the modulus of elasticity and the uniaxial compressive strength of basalt specimens. Prolonged microwave exposure and increased microwave power intensify this reduction in elasticity and strength. Overall, as microwave exposure increases, the specimens exhibit a delayed transition into the elastic stage during uniaxial compression and a more pronounced microcrack compaction stage in the stress–strain curves (Figure 7). The post-peak curves further suggest that microwave radiation enhances the ductility of the specimens, making the post-damage stage more pronounced.

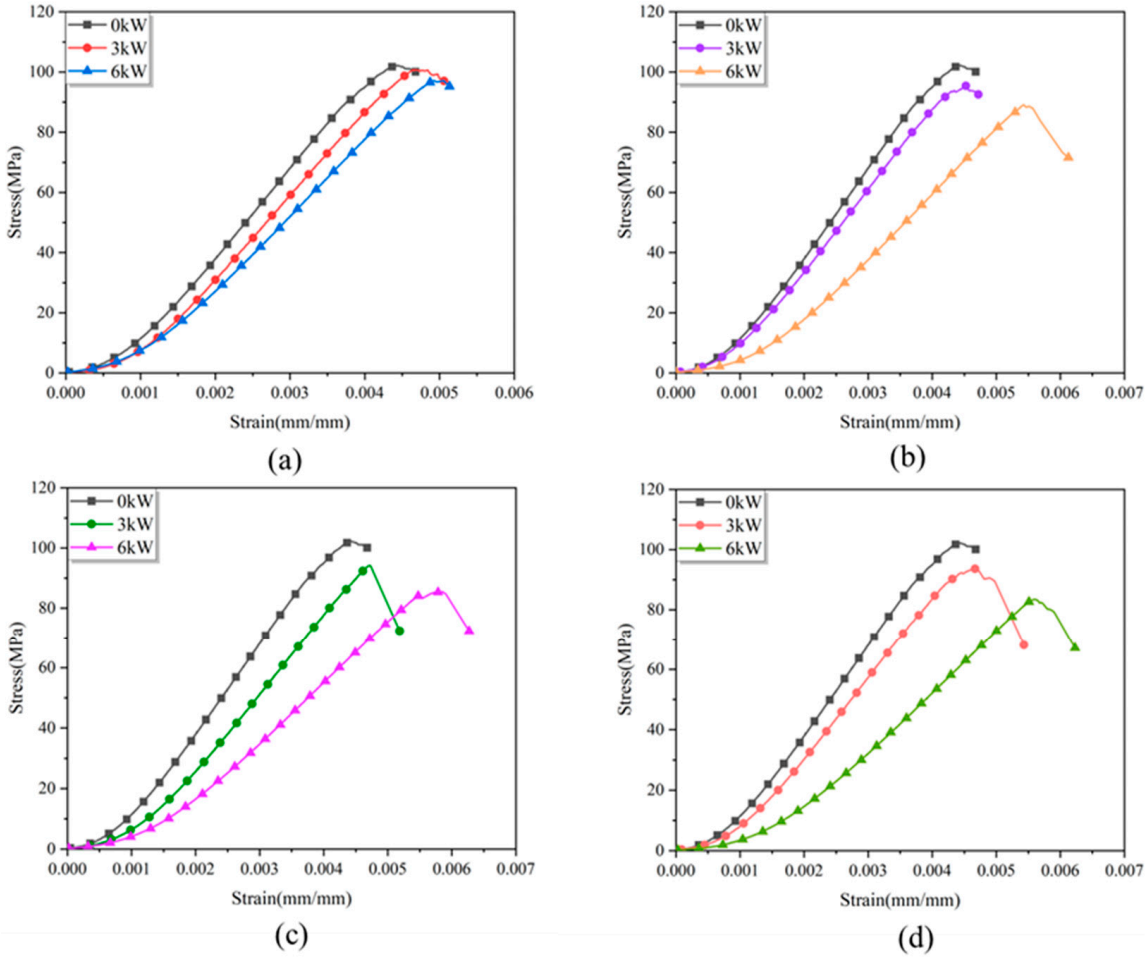

Figure 7. Stress–strain curves of basalt after microwave irradiation. (**a**) The microwave radiation time is 30 s. (**b**) The microwave radiation time is 60 s. (**c**) The microwave radiation time is 90 s. (**d**) The microwave radiation time is 120 s.

Table 4. The main mechanical parameters of basalt specimens under different microwave radiation power and time.

Microwave Power	Radiation Duration	Peak Axial Stress, σ_c/(MPa)	Modulus of Elasticity, E/(GPa)
0 kW	0 s	102.25	30.31
3 kW	30 s	100.78	28.22
	60 s	95.43	26.88
	90 s	94.10	26.78
	120 s	93.72	26.49
6 kW	30 s	97.20	26.15
	60 s	89.07	21.86
	90 s	85.55	20.60
	120 s	83.49	19.94

3.4. Laws of Energy Evolution During Uniaxial Compression of Basalt After Microwave Irradiation

Microwave radiation modifies the structural properties of rocks, particularly in terms of porosity and crack formation, which subsequently influences their mechanical behavior. In this study, the damage inflicted on basalt specimens by microwaves is quantitatively assessed by analyzing the strain energy prior to the peak of the specimens' stress–strain curves. The methodology follows the principles of uniaxial loading and unloading experiments, as depicted in Figure 8.

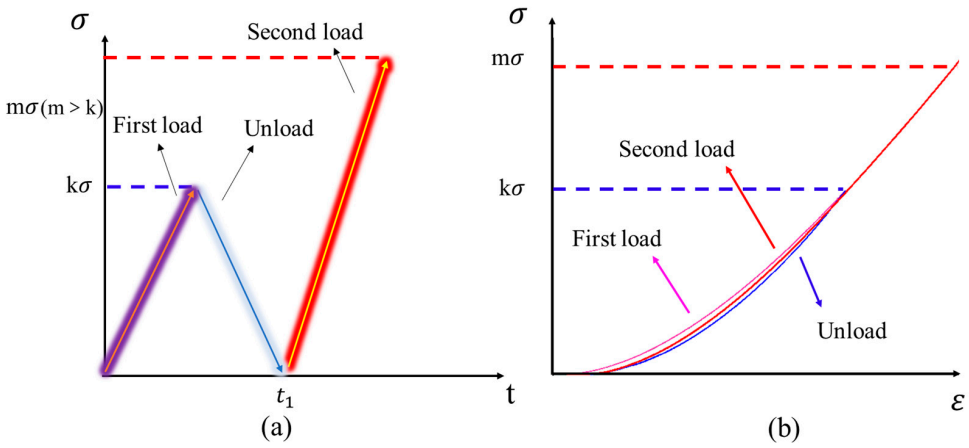

Figure 8. Uniaxial loading and unloading experiment original diagram. (**a**) Stress–time diagram. (**b**) Stress–strain diagram.

The stress–strain curve generated from the uniaxial loading and unloading test mirrors that of the uniaxial compression test up to the unloading point. To quantify the extent of damage, this study measures the elastic strain energy (u_e), dissipation energy (u_d), and total input energy (u_t) of the rock specimens by performing three cycles of loading and unloading on each group of specimens, as illustrated in Figure 9. The calculations for these energy components are based on the following formulas:

$$u_t = \int_0^{\varepsilon_1} f_1(\varepsilon)d\varepsilon \tag{2}$$

$$u_e = \int_{\varepsilon_2}^{\varepsilon_1} f_2(\varepsilon)d\varepsilon \tag{3}$$

$$u_d = u_t - u_e = \int_0^{\varepsilon_1} f_1(\varepsilon)d\varepsilon - \int_{\varepsilon_2}^{\varepsilon_1} f_2(\varepsilon)d\varepsilon \tag{4}$$

where f_1 represents the stress–strain curve of the rock during the initial loading, and f_2 represents the curve obtained by unloading the rock specimen at the unloading point. ε_1 is the strain of the basalt specimen at the unloading point, and ε_2 is the strain of the specimen when the unloading stress reaches zero. The total input energy (u_t), dissipation energy (u_d), and elastic strain energy (u_e) for each uniaxial loading and unloading experiment can be calculated according to the formulas, as shown in Figure 10. Xu et al. [38] posit that an external load is a prerequisite for the accumulation of energy in the rock, and there is a linear relationship between energy storage and external load at different temperatures, which aligns with the law of energy storage:

$$u_e = Au_t + B \tag{5}$$

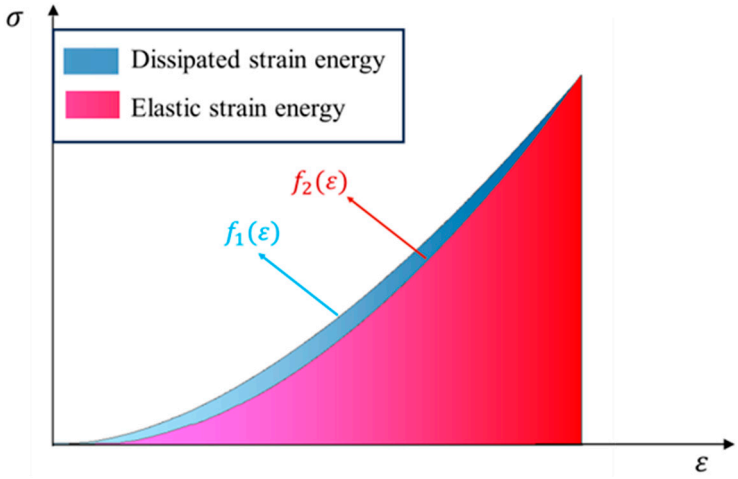

Figure 9. Uniaxial loading and unloading experiment original diagram.

Assuming the same linear relationship between u_e and u_t for basalt under microwave radiation:

$$u_d = Ku_t + M \tag{6}$$

where K is the compression energy dissipation factor, and M is the fitting constant. When the external input energy (u_t) is 0, meaning there is no input energy, u_d (the dissipation energy) must also be 0, which leads to $M = 0$. In this formula, the magnitude of K reflects the energy storage capacity of the specimen. A larger K value indicates that more of the external input energy is converted into dissipative energy, signifying that the specimen's energy storage capacity is weaker, and consequently, the greater the damage the specimen has sustained.

The investigation revealed that the energy storage capacity of rock specimens showed minimal changes after just 30 s of microwave irradiation. As a result, the specimens were divided into seven groups for further analysis of the effects of prolonged exposure times. Loading and unloading experiments were conducted at a rate of 0.1 mm/min, using microwave powers of 3 kW and 6 kW for durations of 0, 60, 90, and 120 s, respectively. The resulting curves, presented in Figure 10, were analyzed through linear fitting to assess the energy characteristics of the basalt. The fitting results indicate a strong linear relationship, supporting the assumed energy storage behavior. As demonstrated in Table 5, under constant microwave power, the longer the duration of microwave radiation, the larger the compression energy dissipation factor K becomes. The increase in K suggests a deterioration in the rock's energy storage capacity, implying that longer radiation times lead to more significant damage to the rock specimens.

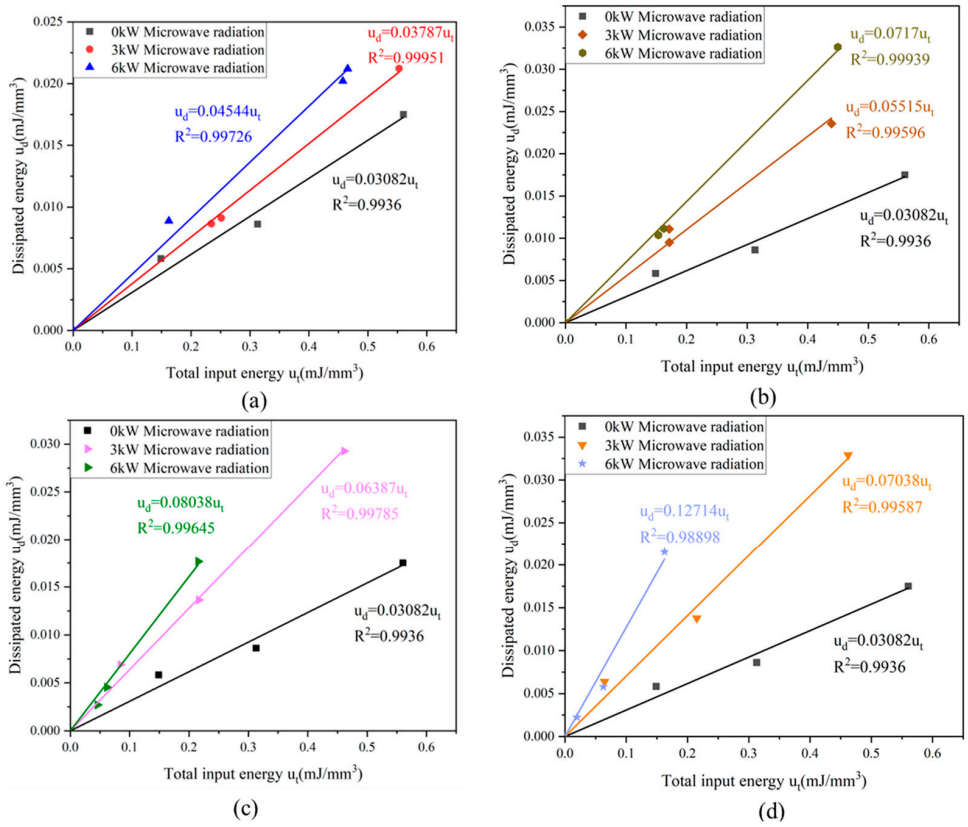

Figure 10. Linear fitting function between u_d and u_t of basalt samples under different microwave radiation times: (**a**) 30 s; (**b**); 60 s; (**c**) 90 s; (**d**) 120 s.

This correlation between prolonged microwave exposure and reduced energy storage capacity underscores the detrimental impact of microwave radiation on the structural integrity of the rocks. Through experimental comparisons, it becomes evident that specimens with lower energy storage capacities sustained more extensive damage due to microwave radiation, affirming the method's effectiveness in assessing the vulnerability of rocks to microwave-induced changes. From Figure 10, it can be observed that both longer microwave radiation times and increased microwave power reduce the energy storage capacity of basalt specimens. This indicates that increasing either the microwave radiation time or the power intensifies the damage to the specimens. Notably, the K-value of basalt after 120 s of 3 kW microwave radiation is smaller than that after 60 s of 6 kW microwave radiation, suggesting that microwave radiation power has a more pronounced effect on reducing the energy storage capacity of basalt specimens than the duration of exposure.

Table 5. Linear fitting function between u_d and u_t of basalt samples after microwave irradiation.

Microwave Power	Radiation Time	Independent Variable	Dependent Variable	*K*	R^2
0 kW	0 s	u_t	u_d	0.03082	0.99360
3 kW	30 s	u_t	u_d	0.03787	0.99951
	60 s	u_t	u_d	0.05515	0.99596
	90 s	u_t	u_d	0.06387	0.99785
	120 s	u_t	u_d	0.07038	0.99581
6 kW	30 s	u_t	u_d	0.04544	0.99726
	60 s	u_t	u_d	0.07170	0.99939
	90 s	u_t	u_d	0.08038	0.99645
	120 s	u_t	u_d	0.12714	0.98898

3.5. Acoustic Emission Testing Based on Uniaxial Experiments

The AE characteristics are closely related to the changes in microstructure and crack behavior within the rock. The closure, expansion, aggregation, and propagation of cracks in basalt specimens during uniaxial loading can be inferred from the acquisition of AE signals. The acoustic emission (AE) characteristics of basalt were evaluated under uniaxial compression. The testing utilized a six-channel acoustic emission (AE) system (model PCI-2) from the Physical Acoustics Corporation (PAC), which was equipped with Mini300 AE sensors. To mitigate background noise interference, a threshold amplitude of 40 dB was set, ensuring that only AE signals with amplitudes above 40 dB were recorded by the transducer. As shown in Figure 11, the AE activity for basalt specimens without microwave radiation is primarily concentrated in the post-peak stage of loading. However, microwave radiation significantly alters this behavior, with AE counts occurring more frequently across all stages of loading in specimens that have undergone microwave radiation. This increase in AE activity can be attributed to the fact that microwave radiation promotes the formation and development of microfractures within the rock. As the microwave radiation time increases, the AE active period of the basalt specimens expands during uniaxial loading. Additionally, higher microwave power further amplifies this effect, resulting in a more pronounced increase in the AE active period compared to lower microwave power. This suggests that both the duration and intensity of microwave radiation significantly contribute to the advancement of microfracture activity within the rock.

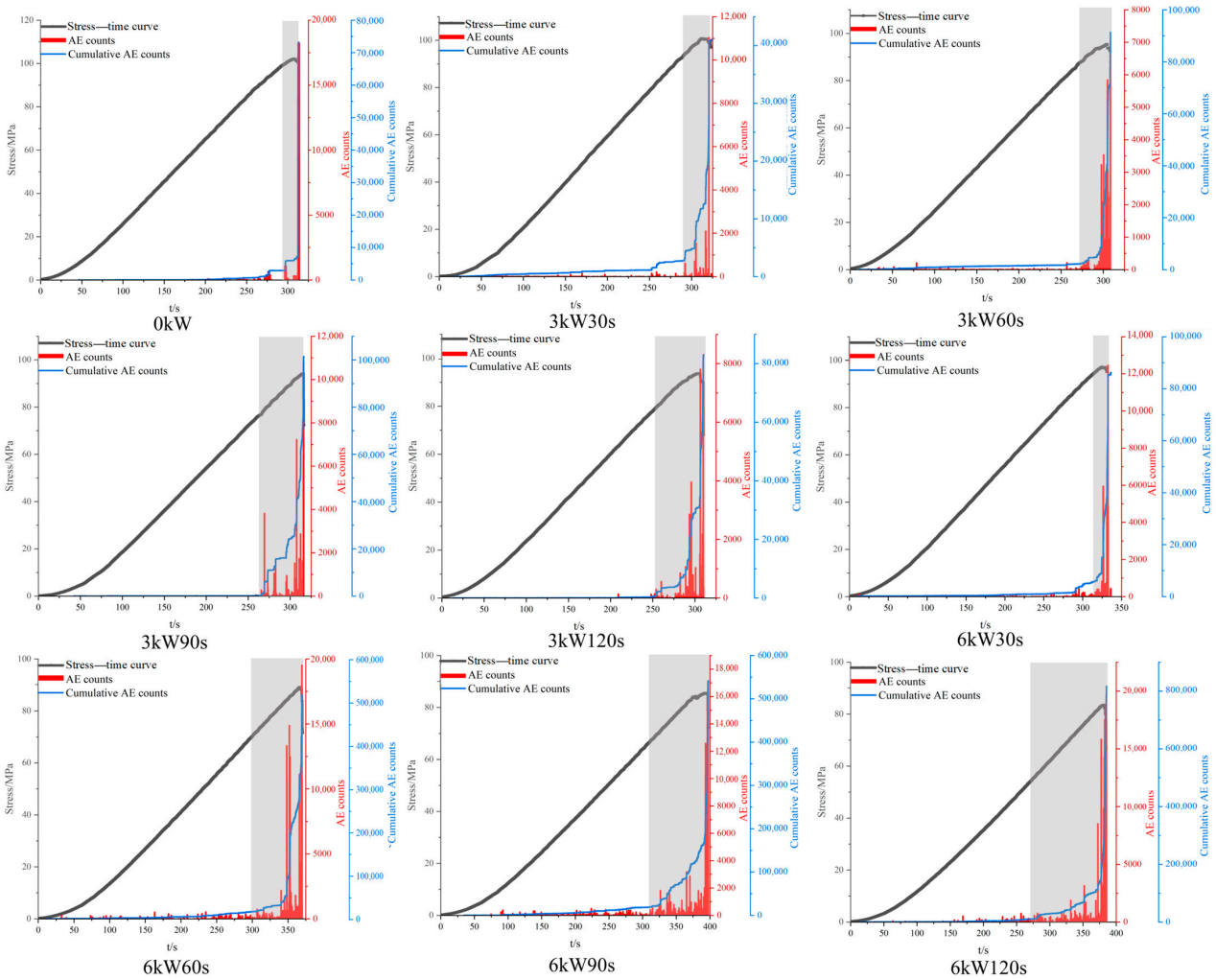

Figure 11. AE counts of basalt specimens under uniaxial loading.

3.6. Transformation of Basalt Crack Types Under Microwave Radiation

During the failure of basalt, the two primary modes of destruction are tensile failure and shear failure. In the formation and propagation of cracks under uniaxial compression, the acoustic emission parameters AF (average frequency) and RA (rise time to amplitude ratio) can reflect the types of cracks and are used to characterize them [39]. The values of AF and RA were obtained by analyzing and summarizing the waveforms of acoustic emission signals from basalt after microwave radiation, as shown in Figure 12. The formulas for these two acoustic emission parameters are as follows:

$$AF = \frac{Count}{Duration} \tag{7}$$

$$RA = \frac{Rise}{Amplitude} \tag{8}$$

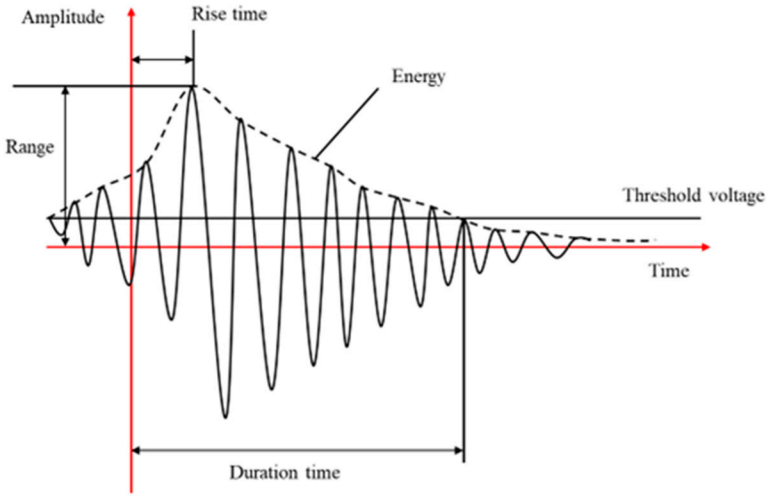

Figure 12. Acoustic emission waveform parameter definition.

To better understand the fragmentation mechanism of basalt after exposure to varying levels of microwave radiation, the normalized AF and RA values are presented in Figure 13. When the RA value is low and the AF value is high, it indicates tensile damage and the formation of tensile cracks. Conversely, when the RA value is high and the AF value is low, it suggests shear damage and the generation of shear cracks. The experimental results demonstrate that extending the microwave radiation time and increasing the microwave radiation power led to a higher proportion of tensile cracks in basalt during uniaxial compression, as presented in Table 6. Additionally, the range of RA and AF values expanded with prolonged microwave radiation, indicating that microwave exposure created more microfractures within the basalt, making it more fragmented and fragile. This further confirms that microwave radiation damages basalt by altering its internal microstructure and stress distribution.

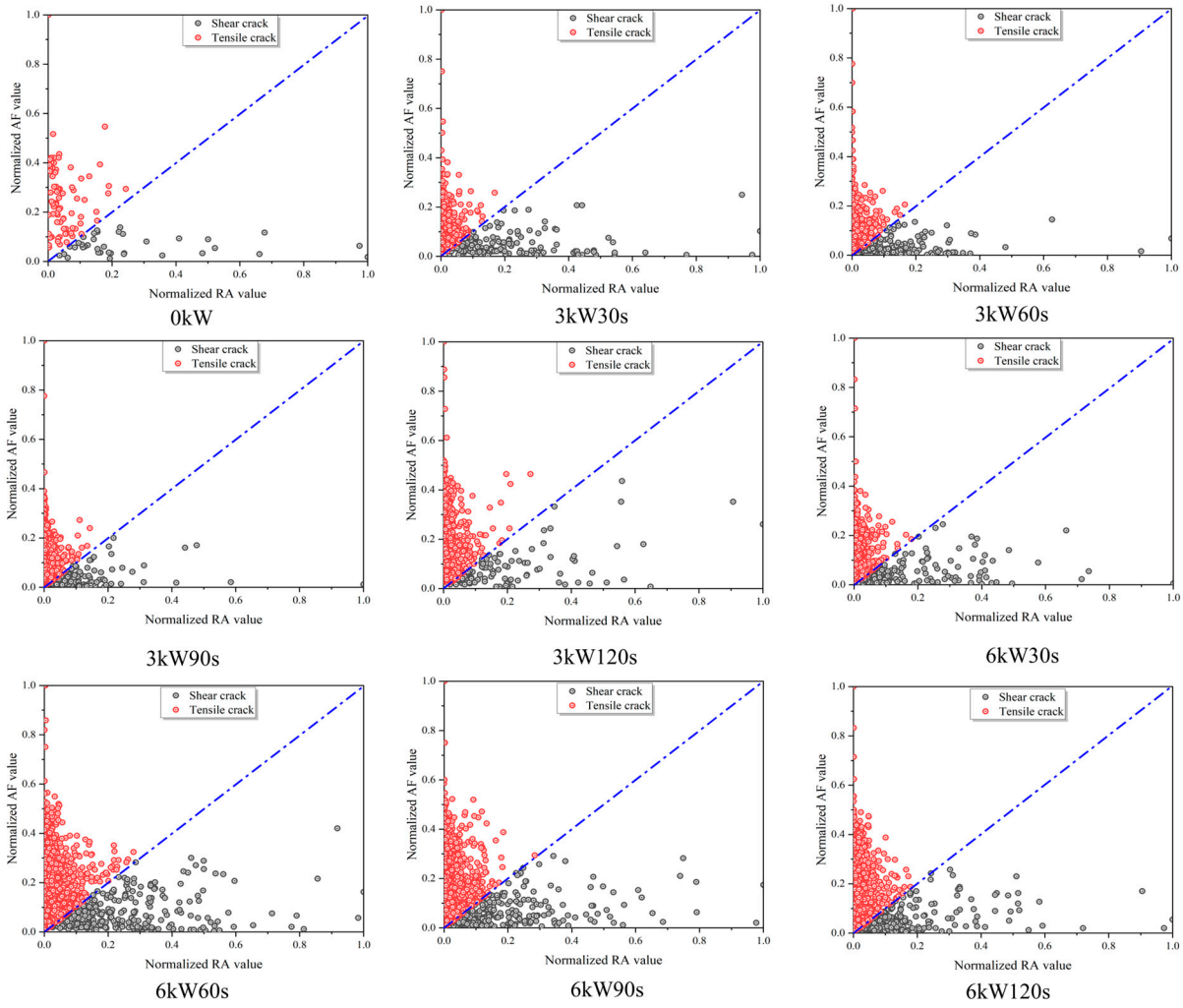

(**a**)

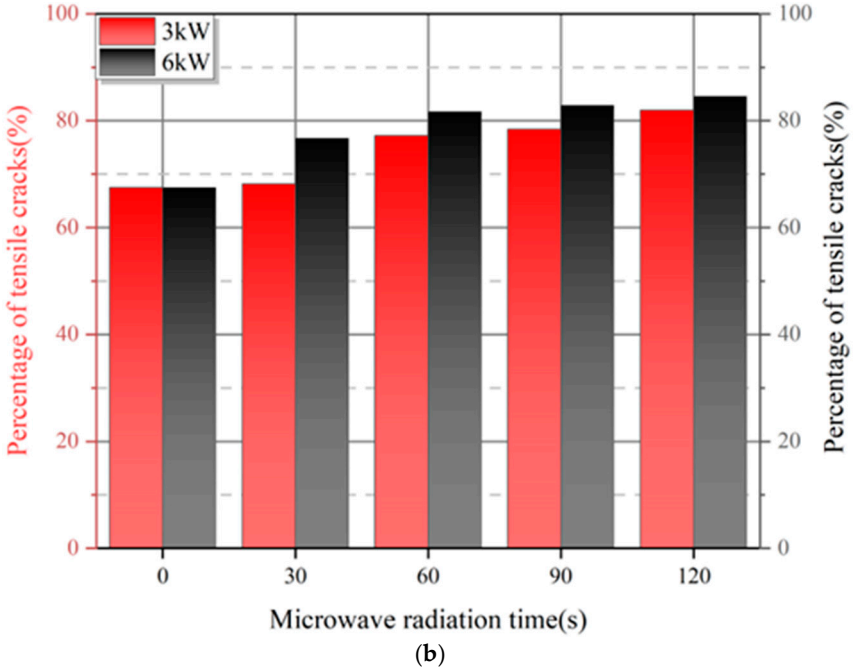

(**b**)

Figure 13. Determination based on RA-AF microcrack cracking mechanism. (**a**) Normalized RA and AF values of basalt under uniaxial load. (**b**) The percentage of tensile cracks in basalt after different microwave radiation.

Table 6. Proportion of basalt tensile and shear cracks exposed to different microwave radiation in uniaxial compression experiments.

Microwave Radiant Power	Microwave Radiation Duration	Percentage of Shear Cracks	Percentage of Tensile Cracks
0 kW	0 s	32.5%	67.5%
3 kW	30 s	32.8%	68.2%
	60 s	22.8%	77.2%
	90 s	21.6%	78.4%
	120 s	18.0%	82.0%
6 kW	30 s	23.3%	76.7%
	60 s	18.3%	81.7%
	90 s	17.1%	82.9%
	120 s	15.4%	84.6%

4. Discussion

4.1. NMR-Based Pore Fractal Modelling

The damage to basalt caused by microwave radiation can be assessed by examining the pore size distribution through the concept of fractal dimension. The fractal dimension quantifies the complexity of the pore structure. A lower fractal dimension indicates that the pores are more evenly distributed, suggesting less damage to the rock. Conversely, a higher fractal dimension points to a more irregular pore structure, often resulting from significant microwave-induced damage. This irregularity may arise from intense heating, which leads to larger or more interconnected pores. Pfeifer et al. [40] describe that fractal structures exhibit self-similarity, meaning they follow a power–law relationship between pore size (r) and the number of pores (N). This relationship is mathematically expressed as follows:

$$N = C_1 r^{-D_f} \tag{9}$$

where C_1 is the constant of proportionality, D_f is the fractal dimension of the fractal structure, and r is the scale parameter of the rock, i.e., the pore size. According to the Kozeny–Carman model, the pores in rock can be regarded as a series of capillaries, and the number of capillaries satisfies the following function:

$$N = \frac{V_{pore}(r)}{\pi r^2 L} \tag{10}$$

where V_{pore} is the total volume of pores in the rock, and r and L are the radius and length of the capillaries, respectively. For simplicity, $L = C_2 r$. Combined with Equation (10), the total volume of pores can also be expressed as follows:

$$V_{pore} = C\pi r^{3-D_f} \tag{11}$$

In addition, the following relationships can be easily deduced:

$$\frac{dV_{pore}}{dr} = C(3 - D_f)\pi r^{2-D_f} \tag{12}$$

Therefore, the cumulative volume of pores in a rock sample with a radius less than r can be described as follows:

$$V_{pore}(< r) = \int_{r_{min}}^{r} C\left(3 - D_f\right)\pi r^{2-D_f} dr = C\pi(r^{3-D_f} - r_{min}^{3-D_f}) \tag{13}$$

where r_{min} is the radius of the smallest pore. Similarly, it is easy to obtain the following relationship:

$$V_{pore}(< r_{max}) = C\pi(r_{max}^{3-D_f} - r_{min}^{3-D_f}) \tag{14}$$

where r_{max} is the radius of the largest pore. Combining Equations (13) and (14) gives Equation (15):

$$\frac{V_{pore}(< r)}{V_{pore}(< r_{max})} = \frac{r^{3-D_f} - r_{min}^{3-D_f}}{r_{max}^{3-D_f} - r_{min}^{3-D_f}} = \frac{\left(\frac{r}{r_{max}}\right)^{3-D_f} - \left(\frac{r_{min}}{r_{max}}\right)^{3-D_f}}{1 - \left(\frac{r_{min}}{r_{max}}\right)^{3-D_f}} \tag{15}$$

When r_{min} is much smaller than r_{max}, combining Equations (14) and (15), the further calculation can be simplified as follows:

$$\frac{V_{pore}(< r)}{V_{pore}(< r_{max})} = (\frac{r}{r_{max}})^{3-D_f} = (\frac{T_2}{T_{2max}})^{3-D_f} \tag{16}$$

$$\frac{V_{pore}(< r)}{V_{pore}(< r_{max})} = \frac{\varphi_{acc}(T_2)}{\varphi_N} \tag{17}$$

Thus, it is easy to obtain Equation (18):

$$\ln(\varphi_{acc}(T_2)) - \ln(\varphi_N) = \left(3 - D_f\right) \ln(\frac{T_2}{T_{2max}}) \tag{18}$$

The fractal dimension of pores within basalt specimens subjected to microwave radiation offers a detailed understanding of the structural changes induced by the treatment. Equation (18), which likely outlines a method for calculating fractal dimensions, was applied to analyze the pore structures using NMR-derived T_2 relaxation times. The resulting data, visualized in Figure 14, revealed significant insights regarding the pore size distribution and fractal characteristics.

From the analysis depicted in Figure 14, it is evident that the relationship between $\ln(\varphi_{acc}(T_2))$ and $\ln(T_2/T_{2max})$ for both the fractal dimension of small pores (D_A) and the fractal dimension of all pores (D_T) did not correspond with the regression model provided by Equation (18). This deviation from the expected regression indicates that the fractal characteristics of both small and overall pore distributions in microwave-treated specimens are not well defined. In other words, the distribution and connectivity of these pores do not exhibit clear self-similar fractal patterns, which are typically described by the power–law relationship associated with fractal structures. This suggests a more chaotic or irregular pore structure, likely caused by the heterogeneous heating effects and localized stresses induced by microwave radiation.

Conversely, the fractal characteristics of large pores (D_P), representing the larger voids and gaps created as smaller pores merge and expand, showed a much better fit to the fractal model, as shown in Table 7. This suggests that the larger voids within microwave-treated basalt specimens exhibit more pronounced fractal behavior, likely due to the coalescence of smaller cracks and voids into larger, self-similar structures. The overall increase in the macroporous fractal dimension D_P indicates that longer microwave radiation durations and higher microwave power promote the formation of these larger fractal pore structures. This can be attributed to the increased energy input from microwave radiation, which amplifies thermal stresses and drives significant microstructural changes within the rock. These alterations in pore structure largely contribute to the inhomogeneity of pore size distribution in basalt specimens. As pores enlarge or new pores form, especially at specific

size levels (with pore diameters greater than 0.1 μm), the uniformity of pore size distribution is disrupted, leading to a wider range of pore sizes and a more heterogeneous distribution. This heterogeneity in pore size affects the rock's physical properties, including permeability, strength, and overall structural integrity.

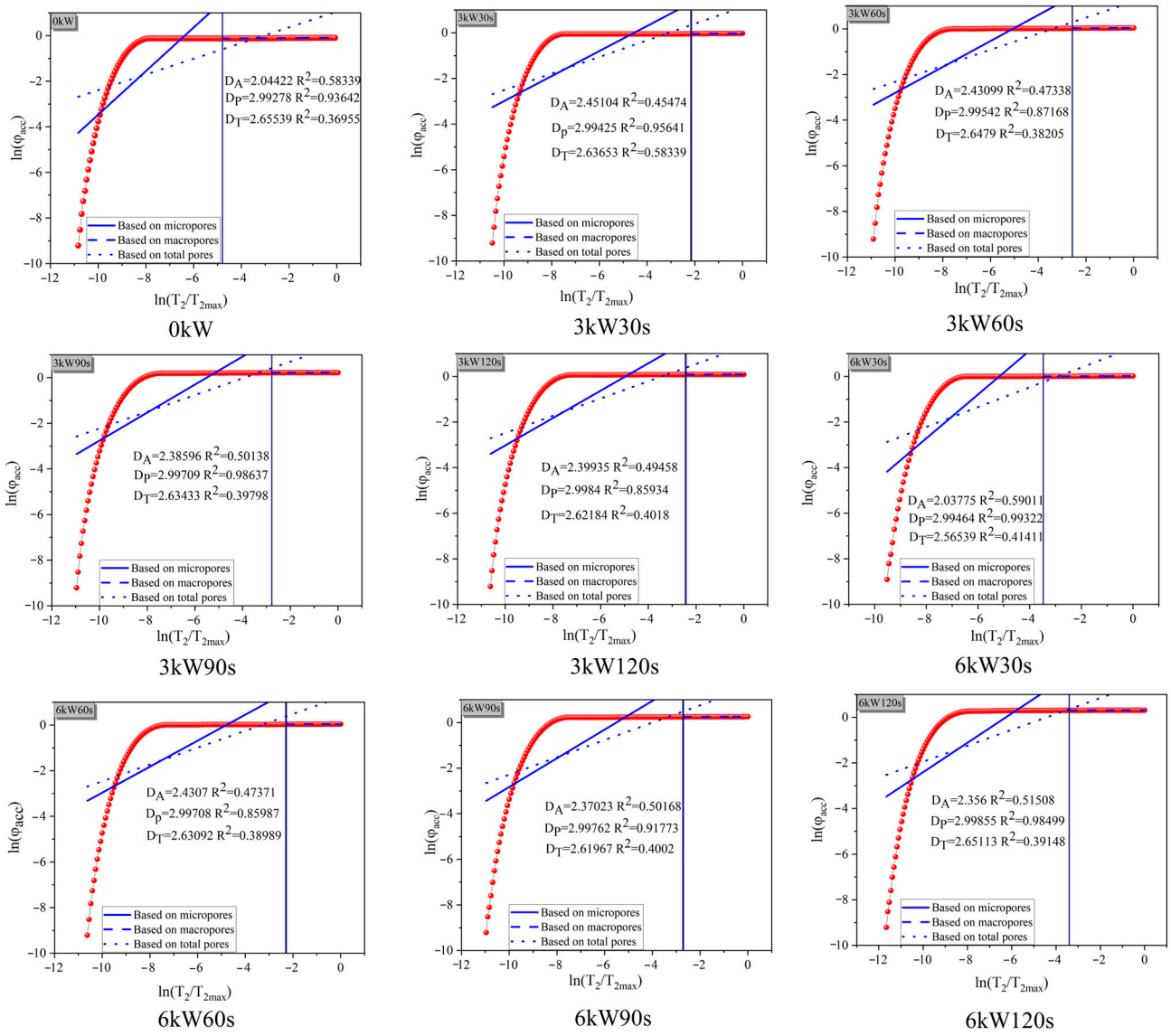

Figure 14. Fractal characteristics of basalt pore structure after microwave treatment.

Table 7. Fractal characteristics of basalt pore structure after microwave treatment.

Microwave Power	Radiation Duration	Macroporous Fractal Dimension D_P	R^2
0 kW	0 s	2.99278	0.93642
3 kW	30 s	2.99425	0.95641
	60 s	2.99542	0.87168
	90 s	2.99709	0.98637
	120 s	2.99840	0.85934
6 kW	30 s	2.99464	0.99322
	60 s	2.99708	0.85987
	90 s	2.99762	0.91773
	120 s	2.99855	0.98499

4.2. Mechanisms of Damage to Basalt After Microwave Treatment

When using mechanical tools to mine hard rock, severe wear and tear on the tools and high economic costs present major challenges that hinder efficient mining. Pre-destruction of hard rock using microwaves can offer a more effective solution to this problem. Microwave power and irradiation time are the primary factors contributing to the deterioration of rock properties, mainly due to the uneven contraction and expansion of minerals caused by differences in their microwave absorptivity and thermal expansion coefficients [41,42]. After microwave radiation, the temperature of strongly absorbing minerals rises significantly higher than that of weakly absorbing minerals, creating a temperature gradient within the rock. As previously mentioned, higher microwave power and longer irradiation times lead to a more pronounced weakening of the physical and mechanical properties of basalt. Notably, microwave power has a greater impact on the extent of internal damage to basalt compared to irradiation time. Additionally, as shown in Table 4, the damage rate from microwave radiation on basalt initially increases and then decreases over time. This occurs because microwave power directly influences the maximum temperature gradient inside the rock. In the early stages of radiation, the temperature difference between minerals increases, accelerating the development of cracks. However, as radiation time extends, heat transfer reduces the temperature gradient, slowing the formation and growth of cracks within the rock. The microscopic damage mechanism is illustrated in Figure 15. Therefore, in practical ore mining, selecting the appropriate microwave power and irradiation time can enhance both economic efficiency and mining productivity. This insight highlights the potential for applying microwave-assisted rock breaking in mining operations [43].

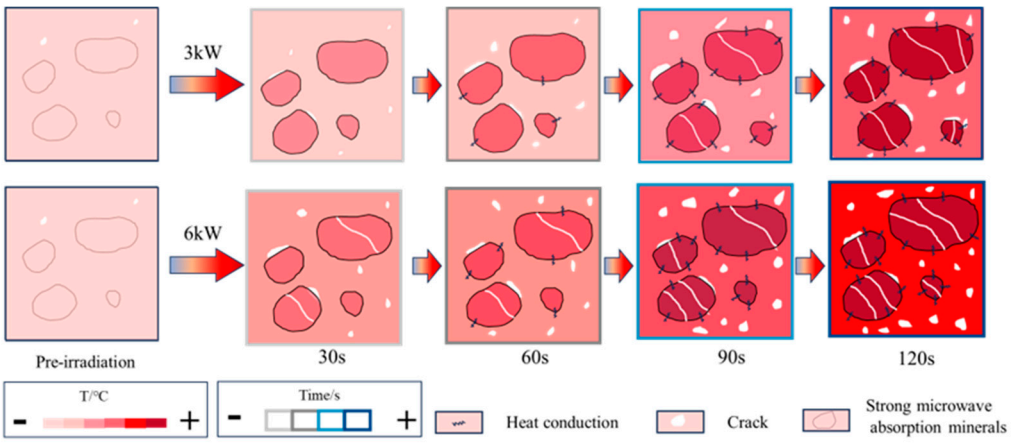

Figure 15. Schematic diagram of the mechanism of basalt damage after microwave treatment.

5. Conclusions

In this paper, based on uniaxial compression experiments and nuclear magnetic resonance (NMR) experiments, we quantitatively analyzed the damage mechanisms and progression of microwaves on basalt from both macroscopic and microscopic perspectives:

(1) Through uniaxial loading and unloading experiments, we demonstrated that the energy storage capacity of basalt specimens before peak stress diminishes with increased microwave radiation power and irradiation time. As a result, a larger proportion of the input energy from the testing machine is converted into dissipated energy, leading to more extensive damage to the specimens.

(2) Under 3 kW of microwave radiation, the damage coefficient F_D of the specimen after 30 s of irradiation is only 29.89% of that after 60 s, while the damage coefficient after 90 s reaches 85.25% of that after 120 s. Similarly, under 6 kW of microwave radiation, the damage coefficient after 30 s is 36.93% of that after 60 s, and the damage coefficient

after 90 s reaches 94.51% of that after 120 s. These findings highlight the progressive nature of damage accumulation with longer irradiation times, with higher power settings accelerating the damage process. Moreover, the extent of damage follows a pattern where the rate of damage initially increases and then decreases as radiation time is extended. In practical rock-breaking engineering applications, it is advisable that the exposure duration for 3 kW and 6 kW microwave radiation should not exceed 90 s; otherwise, the project may become economically unfeasible.

(3) In the uniaxial loading experiments, we incorporated acoustic emission (AE) testing. The results revealed that the AE counts of basalt specimens increased with prolonged microwave radiation. Simultaneously, the ratio of shear cracks to the total number of cracks within the specimens increased with irradiation time.

(4) Using nuclear magnetic resonance (NMR) to analyze porosity and pore distribution, we observed that microwave treatment significantly increases the porosity of basalt, indicating the expansion of existing pores and the formation of new fractures. Fractal analysis of the pores via linear regression suggests that the fractal dimension of macropores increases with extended microwave exposure. This indicates that microwave radiation not only enlarges existing pores but also encourages the formation of new ones, resulting in a more complex pore structure within the basalt.

Author Contributions: T.Y.: Conceptualization, Data curation, Formal analysis, Investigation, Funding acquisition, Resources, Writing—original draft, Writing—review and editing. J.W.: Conceptualization, Data curation, Formal analysis, Investigation, Methodology, Validation, Writing—original draft, Writing—review and editing. J.M.: Investigation, Validation. J.L.: Investigation, Validation. H.D.: Investigation, Validation. All authors have read and agreed to the published version of the manuscript.

Funding: This work was financially supported by the Natural Science Foundation of Hunan Province (2023JJ30662) and Fundamental Research Funds for the Central Universities of Central South University (2024ZZTS0701). We also thank the anonymous reviewers for their valuable comments and suggestions for improving this manuscript.

Data Availability Statement: The data presented in this study are available on request from the corresponding author.

Conflicts of Interest: We declare that we have no financial or personal relationships with other people or organizations that could inappropriately influence our work. There are no professional or other personal interests of any nature or kind in any product, service, and/or company that could be construed as influencing the position presented in, or the review of, the manuscript entitled.

References

1. Cao, X. Regulating mine land reclamation in developing countries: The case of China. *Land Use Policy* **2007**, *24*, 472–483. [CrossRef]
2. Li, B.Y.; Zhou, N.; Qi, W.Y.; Li, A.L.; Cui, Z.Z. Surface Subsidence Control during Deep Backfill Coal Mining: A Case Study. *Adv. Civ. Eng.* **2020**, *2020*, 6876453. [CrossRef]
3. Zhou, H.W.; Xie, S.L.; Jia, W.H.; Zhao, J.W.; Sun, X.T.; Yang, S.; Wei, Q.; Wang, X.Y. Coal permeability considering mining-induced stresses subjected to fractional derivative. *Geomech. Energy Environ.* **2022**, *32*, 11. [CrossRef]
4. Li, X.B.; Gong, F.Q.; Tao, M.; Dong, L.J.; Du, K.; Ma, C.D.; Zhou, Z.L.; Yin, T.B. Failure mechanism and coupled static-dynamic loading theory in deep hard rock mining: A review. *J. Rock Mech. Geotech. Eng.* **2017**, *9*, 767–782. [CrossRef]
5. Wang, S.F.; Li, X.B.; Wang, S.Y. Three-dimensional mineral grade distribution modelling and longwall mining of an underground bauxite seam. *Int. J. Rock Mech. Min. Sci.* **2018**, *103*, 123–136. [CrossRef]
6. Wang, S.F.; Li, X.B.; Wang, S.Y.; Li, Q.Y.; Chen, C.; Feng, F.; Chen, Y. Three-dimensional orebody modelling and intellectualized longwall mining for stratiform bauxite deposits. *Trans. Nonferrous Met. Soc. China* **2016**, *26*, 2724–2730. [CrossRef]
7. Wang, S.F.; Sun, L.C.; Li, X.B.; Wang, S.Y.; Du, K.; Li, X.; Feng, F. Experimental Investigation of Cuttability Improvement for Hard Rock Fragmentation Using Conical Cutter. *Int. J. Geomech.* **2021**, *21*, 11. [CrossRef]

8. Zhou, Z.L.; Cai, X.; Li, X.B.; Cao, W.Z.; Du, X.M. Dynamic Response and Energy Evolution of Sandstone Under Coupled Static-Dynamic Compression: Insights from Experimental Study into Deep Rock Engineering Applications. *Rock Mech. Rock Eng.* **2020**, *53*, 1305–1331. [CrossRef]
9. Hu, Y.; Li, W.; Chen, X.; Xu, H.; Liu, S. Temporal and spatial evolution characteristics of fracture distribution of floor strata in deep coal seam mining. *Eng. Fail. Anal.* **2022**, *132*, 105931. [CrossRef]
10. Wang, S.; Sun, L.; Li, X.; Zhou, J.; Du, K.; Wang, S.; Khandelwal, M. Experimental investigation and theoretical analysis of indentations on cuboid hard rock using a conical pick under uniaxial lateral stress. *Geomech. Geophys. Geo-Energy Geo-Resour.* **2022**, *8*, 34. [CrossRef]
11. Lu, G.M.; Zhou, J.J.; Zhang, L.M.; Gao, W.Y. Experimental investigation on the influence of microwave exposure on the cutting performance of TBM disc cutter cutting of hard rocks. *Results Eng.* **2021**, *12*, 10. [CrossRef]
12. Akintunde, I.B.; Lindsay, E.E.; Olakanmi, E.O.; Prasad, R.V.S.; Matshediso, B.I.; Motimedi, T.; Botes, A.; Pityana, S.L. Performance evaluation and failure analysis of conical picks used in a Botswana (Ngwato) mine. *Eng. Fail. Anal.* **2023**, *143*, 106872. [CrossRef]
13. Xu, W.P.; Wan, L.R.; Gao, K.D.; Bu, Y.; Xu, M.; Ma, S.H.; Jiang, K. Analysis of the Influence of Surrounding Rock State on Working Performance of Cutting Head in Metal Mining. *Appl. Sci.* **2024**, *14*, 340. [CrossRef]
14. Florea, V.A.; Toderas, M.; Itu, R.B. Assessment Possibilities of the Quality of Mining Equipment and of the Parts Subjected to Intense Wear. *Appl. Sci.* **2023**, *13*, 3740. [CrossRef]
15. Hu, M.; Bai, Y.; Chen, H.; Lu, B.; Bai, J. Engineering characteristics of laser perforation with a high power fiber laser in oil and gas wells. *Infrared Phys. Technol.* **2018**, *92*, 103–108. [CrossRef]
16. Li, M.; Han, B.; Zhang, Q.; Zhang, S.; He, Q. Investigation on rock breaking for sandstone with high power density laser beam. *Optik* **2019**, *180*, 635–647. [CrossRef]
17. Rui, F.; Zhao, G.-F. Experimental and numerical investigation of laser-induced rock damage and the implications for laser-assisted rock cutting. *Int. J. Rock Mech. Min. Sci.* **2021**, *139*, 104653. [CrossRef]
18. Li, M.Y.; Han, B.; Zhang, S.Y.; Wang, Y. Investigation into Laser Perforation of Rock for Petroleum Exploitation. *Lasers Eng.* **2018**, *41*, 73–99.
19. Zheng, Y.L.; Ma, Z.J.; Yang, S.Q.; Zhao, X.B.; He, L.; Li, J.C. A microwave fracturability index (MFI) of hard igneous rocks. *Int. J. Rock Mech. Min. Sci.* **2021**, *138*, 104566. [CrossRef]
20. Hassani, F.; Nekoovaght, P.; Radziszewski, P.; Waters, K. Microwave assisted mechanical rock breaking. In Proceedings of the ISRM Congress, Beijing, China, 12 October 2011; p. ISRM–12CONGRESS-2011-2379.
21. Kingman, S.W.; Jackson, K.; Bradshaw, S.M.; Rowson, N.A.; Greenwood, R. An investigation into the influence of microwave treatment on mineral ore comminution. *Powder Technol.* **2004**, *146*, 176–184. [CrossRef]
22. Lu, G.-M.; Feng, X.-T.; Li, Y.-H.; Hassani, F.; Zhang, X. Experimental Investigation on the Effects of Microwave Treatment on Basalt Heating, Mechanical Strength, and Fragmentation. *Rock Mech. Rock Eng.* **2019**, *52*, 2535–2549. [CrossRef]
23. Lu, G.-M.; Feng, X.-T.; Li, Y.-H.; Zhang, X. The Microwave-Induced Fracturing of Hard Rock. *Rock Mech. Rock Eng.* **2019**, *52*, 3017–3032. [CrossRef]
24. Toifl, M.; Hartlieb, P.; Meisels, R.; Antretter, T.; Kuchar, F. Numerical study of the influence of irradiation parameters on the microwave-induced stresses in granite. *Miner. Eng.* **2017**, *103*, 78–92. [CrossRef]
25. Hartlieb, P.; Leindl, M.; Kuchar, F.; Antretter, T.; Moser, P. Damage of basalt induced by microwave irradiation. *Miner. Eng.* **2012**, *31*, 82–89. [CrossRef]
26. Meisels, R.; Toifl, M.; Hartlieb, P.; Kuchar, F.; Antretter, T. Microwave propagation and absorption and its thermo-mechanical consequences in heterogeneous rocks. *Int. J. Miner. Process.* **2015**, *135*, 40–51. [CrossRef] [PubMed]
27. Jones, D.A.; Kingman, S.W.; Whittles, D.N.; Lowndes, I.S. The influence of microwave energy delivery method on strength reduction in ore samples. *Chem. Eng. Process. Process Intensif.* **2007**, *46*, 291–299. [CrossRef]
28. Monti, T.; Tselev, A.; Udoudo, O.; Ivanov, I.N.; Dodds, C.; Kingman, S.W. High-resolution dielectric characterization of minerals: A step towards understanding the basic interactions between microwaves and rocks. *Int. J. Miner. Process.* **2016**, *151*, 8–21. [CrossRef]
29. John, R.S.; Batchelor, A.R.; Ivanov, D.; Udoudo, O.B.; Jones, D.A.; Dodds, C.; Kingman, S.W. Understanding microwave induced sorting of porphyry copper ores. *Miner. Eng.* **2015**, *84*, 77–87. [CrossRef]
30. Yang, J.-m.; Liu, J.-t.; Guo, H.-c.; Li, Q.-w.; Wang, W. Effect of microwave heating on the mechanical properties and energy dissipation characteristics of hard rock. *Environ. Earth Sci.* **2022**, *81*, 415. [CrossRef]
31. Yin, T.-b.; Jin, F.-y.; Li, Q.; Li, X.-b. Effects of microwave radiation on dynamic compressive properties of basalt. *Trans. Nonferrous Met. Soc. China* **2022**, *32*, 3388–3403. [CrossRef]
32. Kingman, S.W.; Jackson, K.; Cumbane, A.; Bradshaw, S.M.; Rowson, N.A.; Greenwood, R. Recent developments in microwave-assisted comminution. *Int. J. Miner. Process.* **2004**, *74*, 71–83. [CrossRef]
33. Kingman, S.W.; Vorster, W.; Rowson, N.A. The influence of mineralogy on microwave assisted grinding. *Miner. Eng.* **2000**, *13*, 313–327. [CrossRef]

34. Satish, H. Exploring Microwave Assisted Rock Breakage for Possible Space Mining Applications. Master's Thesis, McGill University, Montreal, QC, Canada, 2005.
35. Qin, L.; Wang, P.; Lin, H.F.; Li, S.G.; Zhou, B.; Bai, Y.; Yan, D.J.; Ma, C. Quantitative characterization of the pore volume fractal dimensions for three kinds of liquid nitrogen frozen coal and its enlightenment to coalbed methane exploitation. *Energy* **2023**, *263*, 12. [CrossRef]
36. Hu, G.Z.; Sun, C.; Huang, J.X.; Xu, G.; Zhu, J.Q. Evolution of Shale Microstructure under Microwave Irradiation Stimulation. *Energy Fuels* **2018**, *32*, 11467–11476. [CrossRef]
37. Li, H.; Lin, B.Q.; Yang, W.; Zheng, C.S.; Hong, Y.D.; Gao, Y.B.; Liu, T.; Wu, S.L. Experimental study on the petrophysical variation of different rank coals with microwave treatment. *Int. J. Coal Geol.* **2016**, *154*, 82–91. [CrossRef]
38. Xu, L.; Gong, F.; Liu, Z. Experiments on rockburst proneness of pre-heated granite at different temperatures: Insights from energy storage, dissipation and surplus. *J. Rock Mech. Geotech. Eng.* **2022**, *14*, 1343–1355. [CrossRef]
39. Xu, R.C.; Li, Z.; Jin, Y.D. Brittleness Effect on Acoustic Emission Characteristics of Rocks Based on a New Brittleness Evaluation Index. *Int. J. Geomech.* **2022**, *22*, 12. [CrossRef]
40. Pfeifer, P.; Avnir, D. Chemistry in noninteger dimensions between two and three. I. Fractal theory of heterogeneous surfaces. *J. Chem. Phys.* **1983**, *79*, 3558–3565. [CrossRef]
41. Lu, G.-m.; Li, Y.-h.; Hassani, F.; Zhang, X. The influence of microwave irradiation on thermal properties of main rock-forming minerals. *Appl. Therm. Eng.* **2017**, *112*, 1523–1532. [CrossRef]
42. Zhang, X.W.; Xu, J.H.; Chen, L.; Cao, Y.; Sun, L.; Shaikh, F. Thermal Response and Mechanical Behaviors of Compact Basalts Induced by Microwave Irradiation. *Geofluids* **2022**, *2022*, 6211437. [CrossRef]
43. Yang, Z.; Tao, M.; Memon, M.B.; Zhuang, D.; Zhao, Y. Microwave irradiation-induced deterioration of rock mechanical properties and implications for mechanized hard rock excavation. *J. Rock Mech. Geotech. Eng.* 2024, *in press*. [CrossRef]